ELSEVIER

Alzheimer's & Dementia 9 (2013) 666–676

Alzheimer's & Dementia

[^{18}F]T807, a novel tau positron emission tomography imaging agent for Alzheimer's disease

Chun-Fang Xia, Janna Arteaga, Gang Chen, Umesh Gangadharmath, Luis F. Gomez, Dhanalakshmi Kasi, Chung Lam, Qianwa Liang, Changhui Liu, Vani P. Mocharla, Fanrong Mu, Anjana Sinha, Helen Su, A. Katrin Szardenings, Joseph C. Walsh, Eric Wang, Chul Yu, Wei Zhang, Tieming Zhao, Hartmuth C. Kolb*

Molecular Imaging Biomarker Research, Siemens Medical Solution USA, Inc, Culver City, CA, USA

Abstract

Objective: We wished to develop a highly selective positron emission tomography (PET) imaging agent targeting PHF-tau in human Alzheimer's disease (AD) brains.

Methods: To screen potential tau binders, human AD brain sections were used as a source of native paired helical filament (PHF)-tau and Aβ rather than synthetic tau aggregates or Aβ fibrils generated in vitro to measure the affinity and selectivity of [^{18}F]T807 to tau and Aβ. Brain uptake and biodistribution of [^{18}F]T807 in mice were also tested.

Results: In vitro autoradiography results show that [^{18}F]T807 exhibits strong binding to PHF-tau-positive human brain sections. A dissociation constant (K_d) of [^{18}F]T807 (14.6 nM) was measured using brain sections from the frontal lobe of AD patients. A comparison of autoradiography and double immunohistochemical staining of PHF-tau and Aβ on adjacent sections demonstrated that [^{18}F]T807 binding colocalized with immunoreactive PHF-tau pathology, but did not highlight Aβ plaques. In vivo studies in mice demonstrated that [^{18}F]T807 was able to cross the blood–brain barrier and washed out quickly.

Conclusions: [^{18}F]T807 demonstrates high affinity and selectivity to PHF-tau as well as favorable in vivo properties, making this a promising candidate as an imaging agent for AD.

Keywords: [^{18}F]T807; Tau; Amyloid β; Alzheimer's disease; Imaging; Autoradiography

1. Introduction

The development of diagnostic tools for Alzheimer's disease (AD) is currently an intense area of research. To date, cerebrospinal fluid (CSF) measurements of amyloid β (Aβ) and tau, and Aβ imaging with radioactive tracers, such as ^{11}C-Pittsburg compound B (PiB) and ^{18}F-florbetapir (Amyvid™, Eli Lilly and Company, Indianapolis, IN)) by positron emission tomography (PET) have been used clinically to assess whether a patient might be suffering from amyloid-related dementia, such as AD. Interestingly, the CSF levels of $A\beta_{42}$ are commonly decreased in AD patients [1] and do not correlate well with disease duration and severity [2]. This test is limited by the lack of standardization for Aβ quantification and spatial information of these aggregates in the brain. Shaw and colleagues [3] demonstrated that increased CSF tau levels appear to correlate with clinical AD disease severity. Higher concentrations associate with greater cognitive impairment in patients with AD compared with cognitively normal individuals [3]. However, this biomarker also has been reported to be stable during the progression of AD, so the use of CSF tau levels as a biomarker for AD is still controversial [4]. The presence of tau in the CSF in AD patients is thought to originate from degenerating neurons and its subsequent diffusion into the CSF [5]. However, increases in CSF tau can also be seen in other neurodegenerative disorders such as frontotemporal dementia, stroke, and Creutzfeldt-Jakob disease [6].

*Corresponding author. Tel.: +1-310-804-7324; Fax: +1-310-744-4879.

E-mail address: hckolb@me.com

1552-5260/$ - see front matter © 2013 The Alzheimer's Association. All rights reserved.
http://dx.doi.org/10.1016/j.jalz.2012.11.008

Rather than measuring aggregated tau or Aβ levels in the CSF, the quantitative and spatial assessment of these lesions in human brains by PET imaging with appropriate paired helical filament (PHF)-tau or Aβ tracers appear to be more useful for the diagnosis, assessment of disease progression, and response to therapy in AD patients. During the past decade, significant progress has been made in the discovery and development of radioactive tracers that target Aβ plaques in AD patients, such as [^{11}C] Pittsburgh Compound B (PiB) [7], 2-(1-{6-[(2-[F]Fluoroethyl)(methyl)amino]-2-naphthyl}ethylidene) malononitrile {[^{18}F]FDDNP} [8], [^{11}C]AZD2184 [9], [^{11}C]SB-13 [10], [^{18}F]BAY94-9172 [11], and [^{18}F] Amyvid™ [12]. PET imaging with [^{11}C]-labeled PiB has been one of the early diagnostic tools in AD [13] and is considered the gold standard for Aβ imaging. Studies have shown that nearly all patients diagnosed with dementia of the Alzheimer type are [^{11}C]PiB positive [14,15]. PiB binds with high affinity to fibrillar Aβ in neuritic plaques and cerebral amyloid angiopathy. However, [^{11}C]PiB retention does not change appreciably with AD symptoms [14,16]. Jack and associates [17] also confirmed that Aβ plaque deposition and cognitive impairment are poorly correlated in AD. Human postmortem studies in 14 females indicate that the density of neurofibrillary tangles (NFTs), which are aggregates of PHF-tau, but not Aβ plaque deposition, correlates with neurodegeneration and cognitive impairment [18].

Although many PET tracers for Aβ plaques have been developed, only a few compounds targeting NFTs have been reported. Fodero-Tavoletti and coworkers [19] reported ^{18}F-THK523 as a tau imaging ligand for AD. They claim that ^{18}F-THK523 binds to tau with high affinity and selectivity over Aβ plaques. However, an independent study by Zeng and colleagues [20] demonstrates that [^{3}H]THK523 binds to NFTs as well as to Aβ plaques in human AD brain sections. In transgenic mouse brain sections, [^{3}H]THK523 binds only to Aβ but fails to bind to NFTs [20]. These findings were confirmed by our own evaluation of [^{18}F]THK523; the tracer binds to both Aβ plaques and PHF-tau in addition to high white matter binding in human AD brain sections (data not shown).

Recently, we published results for another tau PET imaging agent from a different chemical class of compounds, [^{18}F]T808. Although both [^{18}F]T807 and [^{18}F]T808 show excellent selectivity and binding to PHF-tau, they have different pharmacological and in vivo properties, such as metabolism and biodistribution, particularly in the brain [21]. Both agents are currently in profiles phase 0 clinical studies to investigate their potential as imaging agents for AD in humans.

Even though the phosphorylation of tau, which then leads to the formation of PHF-tau, is currently hypothesized to be a downstream product of Aβ toxicity, it is clear that tau pathology alone can cause neurodegeneration, as exemplified by familial and sporadic tauopathies in animal models [22–24] and in elderly humans followed longitudinally [25]. A number of studies have suggested that senile plaques and NFTs occur separately in the brain both temporally [26] and spatially [27]. NFT deposition in the entorhinal cortex is related closely with neuronal loss in the early stages of AD [28,29]. Neurofibrillary lesions develop at specific high-risk sites, and follow a highly characteristic pattern with regard to affected cell types, cell layers, and brain regions, with only minor interindividual variations [30]. Thus, the distribution pattern and density evaluation of aggregated tau in brain could be a very helpful tool for diagnosis and prognosis of AD.

Thioflavin S is a commonly used fluorescent probe for cross-β-sheet conformation in tau compound screening [31,32]. At the beginning of our research, many attempts were made to use the binding of synthetic tau fibrils to thioflavin S for screening of compound libraries. The hit compounds obtained from this screening process were labeled with fluorine-18 ([^{18}F]) and were evaluated further by autoradiography assay using brain tissues. However, the compounds showing high affinity to synthetic tau fibrils exhibited very little or no binding to native tau aggregates in human brain sections. This study demonstrates that induced synthetic tau fibrils are not a reliable surrogate. This is consistent with the findings by others who report heparin-induced PHF-tau are different in size, morphology, and architecture from isolated PHF-tau from AD brain tissues [33]. Thus, in our study, a series of assays was developed using intact brain tissue sections and in vitro autoradiographs to estimate the binding of a tracer to PHF-tau. This native target-based assay process proved to be highly effective and reliable in the evaluation of our tau radioligands.

In this study, we designed and prepared a novel class of 5H-pyrido[4,3-b]indoles and examined their binding affinity toward tau and selectivity over Aβ. Selected compounds were then labeled with [^{18}F] and were evaluated further in a series of in vitro and in vivo assays. We report the in vitro and in vivo preclinical characterization of the lead tracer [^{18}F]T807 as a PET imaging agent for AD.

2. Methods

2.1. Materials

A total of 45 frozen AD and age-matched non-AD human brains were obtained from the National Disease Research Interchange (Philadelphia, PA) and Anatomy Gifts Registry (Hanover, MD). Tau transgenic (APPSWE-Tau, wild type/hemizygous) and background-matched wild-type mice were bought from Taconic (Hudson, NY). Normal mice purchased from Harlan Laboratories (Indianapolis, IN) were used for brain uptake and biodistribution assays. Mouse antihuman PHF-tau (AT-100) and rabbit antihuman $A\beta_{42}$ antibodies were purchased from Thermo Scientific (Rockford, IL). All other chemicals and reagents were purchased from Sigma (St. Louis, MO) or Invitrogen (Carlsbad, CA) unless otherwise stated.

2.2. Brain PHF-tau and Aβ double immunohistochemistry (IHC)

Blocks of brain tissue were cut from the frontal lobe of clinically diagnosed AD patients (33 brains; age, 64–93 years) and age-matched non-AD brains (12 brains; age, 64–89 years). The blocks were embedded in optimal cutting temperature compound and cut into 10-μm sections. To determine the PHF-tau and Aβ load, double IHC of PHF-tau and $A\beta_{42}$ was performed on 10-μm frozen sections. Adjacent sections were used for autoradiography. After fixing in 100% methanol, sections were blocked with 5% goat serum in 0.01 M phosphate buffered saline (PBS) for 1 hour. The sections were then incubated with a mixture of mouse antihuman PHF-tau and rabbit antihuman $A\beta_{42}$ antibodies overnight at 4°C. The PHF-tau or Aβ-positive deposits were visualized by Alexa-594-labeled goat antimouse and Alexa-350-labeled goat antirabbit secondary antibodies (Invitrogen) under an Axio Imager 2 microscope (Carl Zeiss, Inc, Jena, Germany).

PHF-tau and Aβ loads were calculated based on double IHC staining. Fifteen randomly chosen areas from the gray matter under 10× magnification were imaged. Microscope settings were held constant throughout the sampling. Images were then converted to binary using Image J (Version 14.5K, National Institutes of Health, Bethesda, MD). A predetermined threshold value was held constant throughout the analysis. Percent area values were obtained by dividing the area labeled with immunoreactive positive for PHF-tau or $A\beta_{42}$ by the total area in the gray matter. Based on the PHF-tau and Aβ burden, brain sections were divided into three groups (see section 3.2.).

2.3. Fluorescent compound staining with double IHC for PHF-tau and Aβ on human brain sections

T726, a structurally close analog of the lead compound T807, was fluorescent and tested by triple staining (PHF-tau, Aβ, and compound itself) for PHF-tau binding. For staining of tau lesions with fluorescent compounds, sections were quenched after fixation by incubating with 0.25% $KMnO_4$/PBS for 12 minutes prior to washing (water) and neutralized with 0.1% potassium metabisulfite/0.1% oxalic acid/PBS. Sections were then incubated with 100 μM of the test compound in 50% ethanol/PBS for 1 hour at room temperature. Wash with running water for 3 times and rinse in PBS for 5 minutes each for 3 times. After compound staining, sections were blocked in 5% bovine serum albumin in PBS followed by PHF-tau and Aβ double immunostaining as described earlier. Images were visualized on a Zeiss microscope. Colocalization of the compound staining and antibody signals was assessed by overlaying images from each of the stained serial tissue sections.

2.4. [^{18}F]-labeling of T807

Aqueous [^{18}F]fluoride ion was produced on a Siemens RDS 111 cyclotron (tantalum target) and passed through an anion exchange resin cartridge (Machery-Nagel PS-CO3) on an Explora RN automated synthesis module (Synthra GmbH, Hamburg, Germany). The [^{18}F]fluoride ion was eluted from the cartridge using a solution of 3 mg potassium carbonate in 0.4 mL water into a reaction vessel. Kryptofix 222 (20 mg) dissolved in 1 mL acetonitrile was added to the aqueous [^{18}F]fluoride ion mixture in the reaction vessel. The mixture was dried by heating between 68°C and 95°C under a stream of inert gas and/or reduced pressure (250 mbar) to dry the [^{18}F]fluoride. A 1.0-mg solution of the precursor, 7-(6-nitropyridin-3-yl)-5H-pyrido[4,3-b] indole, dissolved in 0.5 ± 0.1 mL anhydrous N,N-Dimethyl sulfoxide (DMSO) was added to the reaction vessel containing the anhydrous [^{18}F]fluoride. The mixture was heated to 130°C for 15 minutes to induce substitution of the $–NO_2$ group by [^{18}F]fluoride. The reaction mixture was cooled to 50°C, and the crude reaction mixture was pushed into another vial containing 90 to 100 mg Fe powder, followed by 1.0 mL formic acid. The mixture was heated to 100°C for 10 minutes, cooled to 50°C, and then 3.5 mL water was added. The crude mixture was filtered and purified via chromatographic separation using a semi-preparative high-performance liquid chromatography (HPLC) column by first washing with 100% H_2O containing 0.1% 12N HCl for 5 minutes. After 5 minutes, the eluent was switched to 18% EtOH: 82% H_2O with 0.1% 12 N HCl. The column effluents were monitored using ultraviolet (254 nm) and radiometric detectors connected in series. The purified [^{18}F]T807 was collected from the column at the retention time window determined for the [^{19}F]T807 reference standard, which coincides with the radiometric detectors. The collected HPLC fraction was diluted with 50 mL sterile water, passed through an activated C-18 cartridge. The cartridge was washed with an additional 10 mL water. The product was eluted with 0.5 mL EtOH, followed with 4.5 mL 21 mM sodium phosphate. The concentration was maintained at equal or less than 50 mCi/mL. When sterile preparations were required, the dose was processed through a 0.22-μm sterile filter into a sterile collection vial.

The average radiochemical yield (decay corrected) was 47%, with a synthesis time of 90 minutes. The average radiochemical purity was > 99%, with an average specific activity of 9.63 Ci/μmol.

2.5. LogP determination of [^{18}F]T807

[^{18}F]T807 (208 μCi) was diluted with 10 mL water. Four aliquots from this sample (200 μL) were put into four separate Eppendorf tubes. These tubes were analyzed on a gamma counter to facilitate the percent recovery calculations. The first tube was segregated as a control sample. The remaining three tubes were spiked with 200 μL 1-octanol, vortexed for 5 minutes, and then centrifuged at 5*g* for 5 minutes. The layers were then separated (top, organic; bottom, aqueous) and put into separate Eppendorf tubes. All the tubes, including the control tube, were analyzed using

a gamma counter. The LogP of T807 is 1.67. The average percent recovery was 100%.

2.6. [^{18}F]T807 autoradiography and correlation with PHF-tau or Aβ IHC

To correlate [^{18}F]T807 binding with PHF-tau and Aβ IHC, autoradiography was performed on adjacent sections from a total 26 AD or age-matched non-AD human brains. Each air-dried frozen section was incubated with 20 μCi [^{18}F]T807 (20 μCi/500 μL per section = 1.92 nM/L) at room temperature for 60 minutes and then washed for 1 minute in PBS, for 2 minutes in 70% ethanol/PBS, for 1 minute in 30% ethanol/PBS, and for 1 minute in PBS to remove unbound tracer. After drying, the labeled section was exposed to a Fuji Bio-Imaging System FLA-7000 (Tokyo, Japan) overnight. Autoradiographic images were obtained and measured using the Multi Gauge program from Fuji (Tokyo, Japan). The correlation between autoradiography signal (intensity from gray matter, which was expressed by ratio of gray matter to white matter) to PHF-tau or Aβ IHC (percent of labeled area vs total area) was determined.

2.7. K_d determination for [^{18}F]T807

Two sets of sections from two brains (from group A and group B) with the same Aβ load (both 0.97% in gray matter) but different PHF-tau deposits (1.17% from group A vs 0.06% from group B) as estimated by IHC were selected for K_d determination using autoradiography. The autoradiographic readings from group A sections were used to determine binding to both PHF-tau and Aβ, and the reading from group B sections was used to determine binding to Aβ only. Thus, the PHF-tau binding of the tracer was obtained by subtracting the group B brain signals from group A brain signals. The Aβ binding of the tracer was obtained from the group B signals. The experiment was set up with 10 adjacent sections from each brain, which had the same PHF-tau or Aβ load by IHC. These 10 pairs of sections were incubated with various concentrations of the tracer (cold T807 from 15–200 nM and [^{18}F]T807 from 3.8 to 50μCi at 10 different concentrations: from 3.8 μCi/500 μL per section–50 μCi/500 μL per section = 0.36, 0.48, 0.64, 0.86, 1.14, 1.52, 2.03, 2.71, 3.61, and 4.82 nM/L). The K_d for T807 was determined by Scatchard plot analysis of the plot drawn between the number of moles of bound ^{18}F compound and the ratio of bound-to-free test compound.

2.8. Brain uptake of [^{18}F]T807 in mice

The purpose of this study was to measure brain penetration of [^{18}F]T807 by dynamic PET imaging in mice. An INVEON multimodality scanner (Siemens, Germany) was used for microPET/computed tomographic imaging. All animal work was performed in accordance to Siemens MIBR Institutional Animal Care & Use Committee–approved procedures. Animals were anesthetized with 3% isoflurane/97% oxygen and placed on a heating pad on the scanner bed. A short high-resolution CT scan was first performed for anatomical registration, followed by a 30-minute PET scan. Within 3 minutes after the beginning of the PET acquisition, [^{18}F]T807 was administered to the animals via tail vein injection (250 μCi in a total volume of 200 μL saline). A PET image was generated for each minute of the acquisition time. Uptake of the tracer was obtained by visually drawing regions of interest based on the fused PET/CT images, and the corresponding activity values were determined using INVEON Research Workplace software (Siemens, Germany). All values are represented as percent injected dose per gram (%ID/g). Six mice were studied in this experiment.

2.9. Biodistribution and excretion of [^{18}F]T807 in mice

Six male mice at each time point were administered 250 μCi [^{18}F]T807 (in 200 μL saline) via tail vein injection. At 5, 15, and 30 minutes after administration, the mice were anesthetized with 3% isofluorane/97% oxygen, and 500-μL whole blood samples were drawn via cardiac puncture and placed immediately into a 1.5-mL tube that was coated with potassium ethylenediamine tetraacetic acid. The anticoagulated blood was centrifuged for 8 minutes at 3000 *g* to separate plasma from red blood cells. After euthanasia, the liver, kidneys, skeletal muscle (right quadriceps), brain, and bone (femur) were harvested and weighed. Each of the tissue samples were transferred to gamma counter tubes and counted on a 1470 Wallac Wizard Gamma Counter (Perkin Elmer, Waltham, MA). Count data were converted to percent injected dose per gram.

2.10. Biostability of [^{18}F]T807 in mice

Six male wild-type mice were administered 300 μCi [^{18}F]T807 (in a maximum volume of 200 μL saline) via tail vein injection. The animals were sacrificed at 10 minutes (n = 3) and 30 minutes (n = 3) postinjection. Whole blood was obtained, weighed, and centrifuged at 3000 *g* for 3 minutes to isolate the plasma. Urine was also collected. The brain, kidneys, and liver were harvested, weighed, and homogenized in lysis buffer (1% sodium dodecylsulfate in PBS buffer). An aliquot of each sample (400 μL) was subsequently removed, mixed with an equal volume of chloroform/methanol (1:1), vortexed, and placed on dry ice. Urine (400 μL) and 800 μL plasma samples were measured and treated with an equal volume of chloroform/methanol (1:1), vortexed, and placed on dry ice for 3 minutes. After thawing, the samples were centrifuged to allow for the separation of organic ($CHCl_3$, bottom layer) and aqueous ($MeOH/H_2O$, top layer) fractions. The organic and aqueous fractions were then removed and assayed for radioactivity in a PerkinElmer Wizard gamma counter (20 seconds). The samples were analyzed by HPLC using a radiometric detector (Raytest GmbH/Agilent).

2.11. Assessment of binding potential to central nervous system (CNS)-relevant receptors, channels, and transporters

Binding of T807 to various CNS receptors and enzymes was tested at Ricerca Biosciences, LLC. Methods used in this study have been adapted from the scientific literature to maximize reliability and reproducibility. Reference standards were run as an integral part of each assay to ensure the validity of the results obtained. Where presented, IC_{50} values were determined by a nonlinear, least squares regression analysis using MathIQ (ID Business Solutions Ltd, UK). Inhibition constants (K_i) are presented. K_i values were calculated using the equation of Cheng and Prusoff [34] based on observed IC_{50} of the tested compound, the concentration of radioligand used in the assay, and the historical values for the K_d of the ligand (obtained experimentally at Ricerca Biosciences, LLC). Where presented, the Hill coefficient (n_H), defining the slope of the competitive binding curve, was calculated using MathIQ. Biochemical assay results are presented as the percent inhibition of specific binding or activity.

3. Results

3.1. Compound screening

In our search for a selective tau binder, we began screening several hundred fluorescent compounds from a number of different chemical classes originally designed to bind to Aβ pathology. Carbazoles were among the chemotypes that yielded potential candidates. Although they did, indeed, show good PHF-tau binding, one concern was that the harmine-type analogs could also be potent monoamine oxidase (MAO) inhibitors. Through several rounds of lead optimization, the fluorescent compound T726 was identified as an early hit that lacked MAO activity and displayed PHF-tau binding properties. T726 demonstrated significant binding to tau aggregates and less binding to amyloid plaques in a triple staining analysis. In Fig. 1, positive T726 staining colocalized with PHF-tau immunostaining of tau tangles, neuropil threads, or neuritic plaques, but not with $Aβ_{42}$ plaques. The purpose of this assay is only to obtain qualitative and topographic information about the test compound, whether it binds to tau and/or Aβ aggregates. A high compound concentration (100 μM) is required because the fluorescence of the compounds is rather weak, and therefore no quantitative measure of the binding affinity is possible. If a compound showed staining of tau tangles, the corresponding radiotracer was prepared for further in vitro and in vivo evaluation. Binding properties to native tau and Aβ were then calculated from autoradiographic results. In vivo (brain uptake in rodents) and in vitro properties were optimized further and a close analog, T807, emerged as a lead candidate. T807, however, does not have any fluorescent properties and therefore could not be visualized directly by

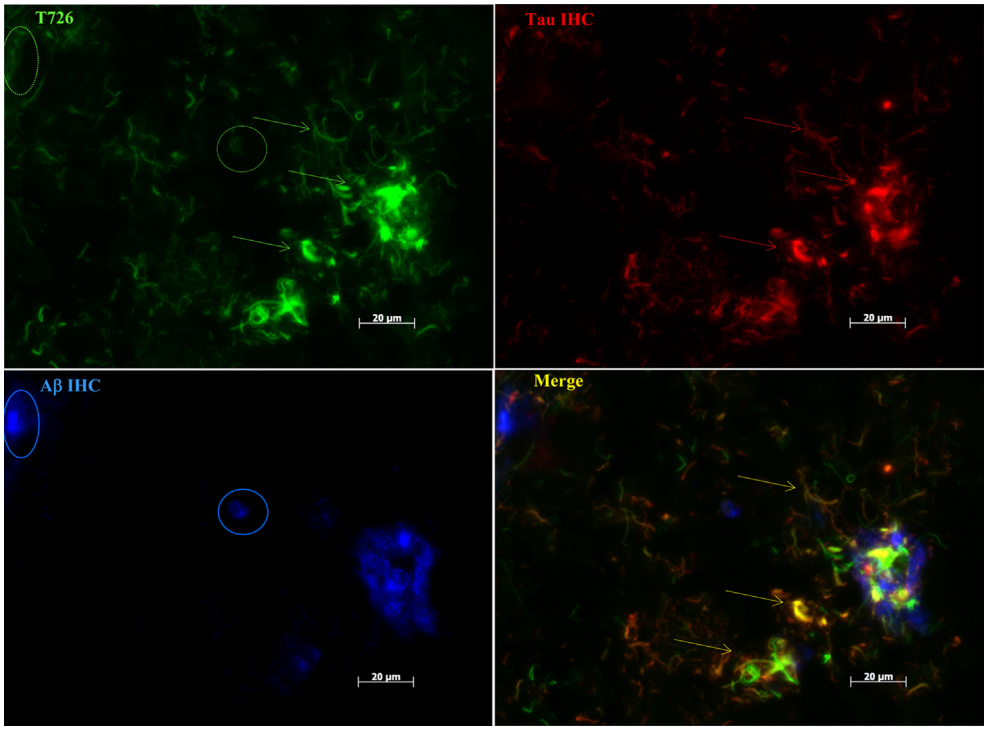

Fig. 1. Colocalization of fluorescent T726 with paired helical filament (PHF)-tau and amyloid beta (Aβ) immunohistochemistry. Microscopic images of a triple-labeled section (10 μm) from the frontal lobe of an Alzheimer's disease brain are presented. The section was immunostained with PHF-tau and $Aβ_{42}$ antibodies as well as 100 μM T726. Arrows indicate the location of tau tangles, neuropil threads, or neuritic plaques and circles indicate amyloid plaques. Positive T726 staining colocalized with PHF-tau immunostaining of tau tangles, neuropil threads, or neuritic plaques, but not with $Aβ_{42}$ plaques. Tissue sections were imaged with a Zeiss Imager 2 microscope and Axiocam digital camera. Scale bars = 20 μm.

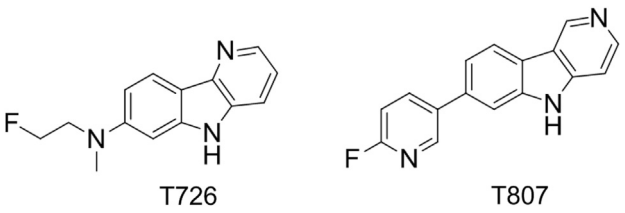

Fig. 2. Chemical structures of T726 (N-(2-fluoroethyl)-N-methyl-5H-pyrido[3,2-b]indol-7-amine) and T807 (7-(6-fluoropyridin-3-yl)-5H-pyrido [4,3-b]indole).

fluorescence microscopy. The chemical structures of T726 and T807 are shown in Fig. 2. Although clearly not identical, the compounds belong to the same class of carbazoles and do compete with each other (data not shown) when the tracer [^{18}F]T807 (20 μCi) and T726 (0.1-5 μM) are incubated together on the same brain section. This serves as further evidence that T807 and T726 occupy the same binding sites.

3.2. PHF-tau and Aβ IHC screening of 45 human brains

Human brain sections from different brains were divided into three groups according to their PHF-tau and Aβ burden as determined by double immunostaining. Group A had PHF-tau and Aβ plaque-rich deposits (both loads $\geq$ 0.3%), group B had poor PHF-tau but Aβ plaque-rich deposits (PHF-tau load $<$ 0.3%, Aβ $\geq$ 0.3%), and group C was negative for both PHF-tau and Aβ plaque deposits (both loads $<$ 0.3%). The clinical diagnosis for the 20 tau-positive brains was AD. Twenty-four of 28 Aβ-positive brains had a clinical diagnosis of AD; the remaining 4 Aβ-positive brains were non-AD cases. Seven of the clinically AD diagnosed brains were not found to have any PHF-tau or Aβ deposits. All the tau-rich brains also had Aβ deposits. We had no brains that were PHF-tau positive and Aβ negative.

3.3. [^{18}F]T807 binds specifically to native PHF-tau aggregates in human brain sections

Autoradiography with [^{18}F]T807 was performed on frontal brain sections that were obtained from 26 brains, including groups A (n = 8), B (n = 9), and C (n = 9). Strong signals in the gray matter from group A were observed, whereas weak or no signals in the cortex regions in group B sections were detected (Fig 3A). The average [^{18}F]T807 binding signal intensity in the gray matter of group A was 25.7 times higher when compared with group B (1018 ± 173 PSL/mm^2 vs 39 ± 15 PSL/mm^2, $P < .001$). Only background autoradiography signals were found on the sections from the normal brains of group C (27 ± 11 PSL/mm^2).

Adjacent brain sections were double immunostained with PHF-tau and Aβ_{42}, and were compared with [^{18}F]T807 autoradiography (Fig. 3B). In all tissue sections examined, positive [^{18}F]T807 signals colocalized with PHF-tau immunostaining, but not with Aβ plaques, as indicated.

The PHF-tau and Aβ loads on adjacent sections from these 26 brains were measured and correlated with autoradiography signals of [^{18}F]T807. These results suggested that [^{18}F]T807 binding correlated with PHF-tau (Fig. 4A) but not with Aβ (Fig. 4B), and further confirmed that [^{18}F]T807 bound to native PHF-tau aggregates of human AD brain with high specificity and weak or no interaction with native Aβ plaques.

3.4. [^{18}F]T807 tau binding affinity measurement

The binding affinities of [^{18}F]T807 to native tau tangles and Aβ were analyzed by saturation binding experiments performed on two sets of brain sections (Fig. 5). The degree of linearity in the Scatchard plot indicated that the binding of the tracer to tau aggregates was well defined within only one type of binding site, which might be the origin of the selectivity of [^{18}F]T807. From the Scatchard analysis, the K_d value for [^{18}F]T807 was determined to be 14.6 nM (Fig. 5B). Because of the heterogeneous nature of the assay, the K_d value is only a relative measure of binding affinity. It cannot be compared directly with published K_d values for amyloid tracers because of these methodological differences. An attempt was also made to determine the K_d value for native amyloid plaques. However, at lower ligand concentrations (<200 nM), the autoradiographic signals were indistinguishable from the background (negative control) as a result of weak binding. At higher concentrations, the binding pattern was highly nonspecific and random. Therefore, a nonlinear regression analysis did not result in a linear function in the Scatchard plot and, as a result, a K_d value for amyloid could not be derived from the kinetic analysis (data not shown). This is yet another indication that [^{18}F]T807 does not bind to Aβ.

3.5. [^{18}F]T807 crosses the blood–brain barrier efficiently

With a low molecular weight (262.1 g/mol), a calculated octanol/water partition coefficient (logP_{oct}) of 3.4 (by ChemBioDraw Ultra 12.0), a measured LogP of 1.67, and a high specific radioactivity of 9.63 Ci/μmol, [^{18}F]T807 should be able to cross the blood–brain barrier and provide good brain PET images. This was confirmed by in vivo PET imaging in mice (n = 6, Fig. 6), which revealed that [^{18}F]T807 displayed rapid brain penetration and fast washout. The average peak percent injected dose per gram of [^{18}F]T807 was 4.16 ± 0.32 at 2 minutes after the injection, and cleared to skeletal muscle levels in about 25 to 30 minutes. The tracer showed some accumulation in the bone, presumably because of defluorination, which results in the release of [^{18}F]fluoride into the blood; however, the bone activity did not increase significantly over time.

3.6. Biodistribution and excretion of [^{18}F]T807 in mice

[^{18}F]T807 cleared rapidly from the brain, with activity values decreasing from 4.43% ID/g at 5 minutes to

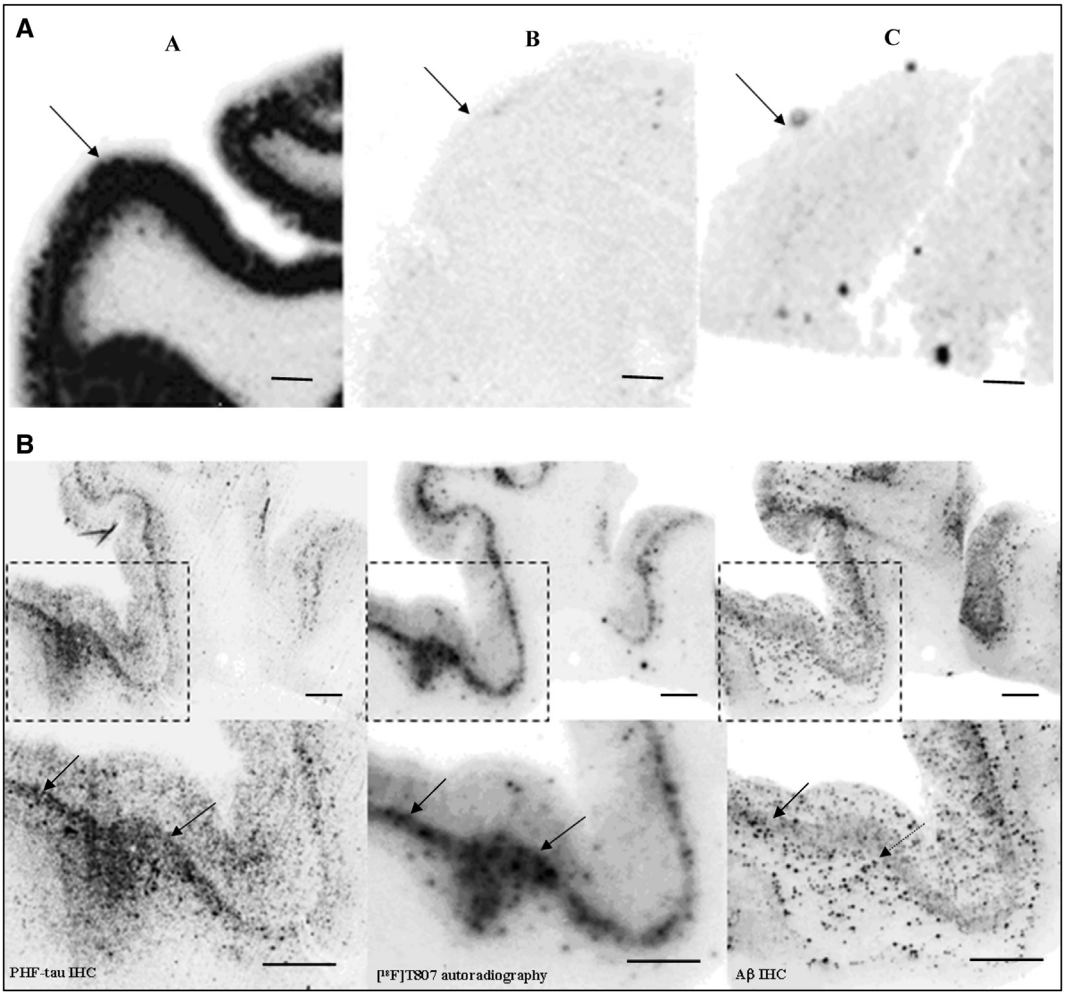

Fig. 3. [^{18}F]T807 autoradiography on brain sections from different groups and its comparison with paired helical filament (PHF)-tau and amyloid beta (Aβ) double immunohistochemistry (IHC). (A) Representative images for [^{18}F]T807 autoradiographs from groups A, B, and C of brains ([^{18}F]T807 autoradiography, 20 μCi/section). Positive autoradiography signals were observed only in the gray matter of brain from the PHF-tau-rich group A. Arrows indicate gray matter. (B) [^{18}F]T807 colocalized with PHF-tau but not with Aβ plaques. (B, top row) Low magnification. (B, bottom row) High magnification from the framed areas. Images of PHF-tau (left) and Aβ (right) IHC double immunostaining and autoradiogram image (middle) from two adjacent sections (10 μm) from a PHF-tau rich group A brain (frontal lobe). Positive [^{18}F]T807 labeling colocalized with immunostaining of PHF-tau but not with Aβ plaques, as indicated by arrows. Fluorescent and autoradiographic images were obtained using a Fuji Film FLA-7000 imaging instrument. Scale bars = 2 mm.

0.62% ID/g at 30 minutes. Kidney elimination was a significant clearance pathway, resulting in a maximum tracer concentration of 14.99% ID/g in the kidneys at 5 minutes, which decreased to 5.52% ID/g at 30 minutes. The accumulation of activity in muscle and bone remained relatively low throughout the PET scan (Table 1).

3.7. Metabolism studies of [^{18}F]T807

The metabolism data are presented as percent of the injected dose per gram of tissue of the organic/aqueous fractions for each organ at the 10-minute and 30-minute time points. Four metabolites were detected, all with shorter retention times than [^{18}F]T807. The total recovery of radioactivity injected onto the analytical HPLC column was calculated to be approximately 70%, using Na^{18}F as the radioactive reporter. The brain percent of the injected dose per gram of [^{18}F]T807 at 10 minutes was 1.15 with no other metabolites present. After 30 minutes, [^{18}F]T807 decreased to 0.32% ID/g with no other metabolites present. In plasma, at 10 minutes, the radioactivity was partitioned 34% (0.03% ID/g) being the parent tracer and the remaining 66% (0.29% ID/g) was metabolite 1, presumed to be [^{18}F] fluoride. No other metabolites were found in plasma. At 30 minutes, the plasma contained a large amount of radioactivity, metabolite 1 presumed to be [^{18}F]fluoride (0.47% ID/g), and a small amount of intact parent compound (0.02% ID/g). In the liver sample at 10 minutes, 78% (3.49% ID/g) parent was present whereas the remaining 22% of activity was comprised of both [^{18}F]fluoride and metabolite 4 present in almost equal amounts of 1.81% ID/g and 1.66% ID/g, respectively. At 30 minutes, the parent tracer's uptake dropped to 2.47% ID/g (30%) along with [^{18}F]fluoride (1.52% ID/g) and metabolites 2, 3, and 4 (0.85% ID/g,

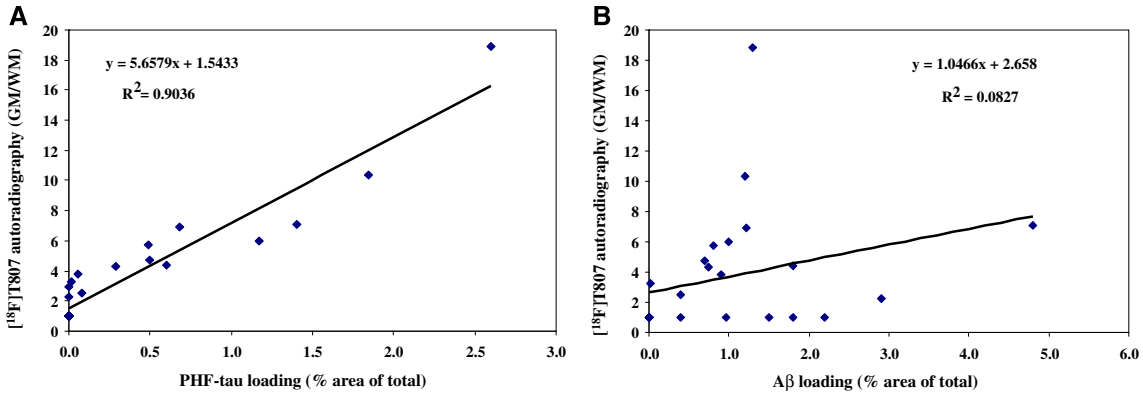

Fig. 4. Correlation between [^{18}F]T807 autoradiography signals and paired helical filament (PHF)-tau or amyloid beta (Aβ) immunohistochemistry (IHC). Two adjacent sections were stained with 20 μCi [^{18}F]T807 or double stained with PHF-tau and Aβ. Twenty-six brains from three groups were measured. PHF-tau IHC and [^{18}F]T807 autoradiography showed linear correlation (A), but no correlation was observed between Aβ IHC and [^{18}F]T807 binding (B). Abbreviation: GM/WM, ratio of grey matter signal vs. white matter signal.

0.52% ID/g, and 2.76 % ID/g, respectively). In the kidney homogenate, the parent tracer was present in higher amounts compared with other tissues (4.19% ID/g) along with metabolite 3 (2.98% ID/g) and a small amount of metabolite 4 (0.61% ID/g). After 30 minutes, the kidney homogenate contained parent with 2.05% ID/g and a small amount of [^{18}F] fluoride (0.36% ID/g) and metabolite 4 (0.61% ID/g). The tracer and the metabolites were cleared predominantly through the kidneys and through urine.

3.8. Assessment of binding potential to CNS-relevant receptors, channels, and transporters

T807 was assessed in competitive binding assays against a panel of 72 of the most common CNS targets. Five targets—human norepinephrine transporter 1, rabbit monoamine transporter, rat glutamate receptor, NDMA, and human μ-opiate—showed inhibition of $>$ 50% at a 10-μM screening concentration. For all other targets, the inhibition of specific binding was low. The IC_{50} of T807 was determined to be 2.2 μM for the norepinephrine transporter, 0.4 μM for the monoamine transporter, and 2.7 μM for the glutamate receptor. The inhibition of the μ-opiate receptor by T807 was assessed further at lower concentrations. The inhibition was 31% of specific binding at 1 μM and 12% at 0.1 μM, and no IC_{50} was determined.

T807 was also assessed in assays for MAO-A, MAO-B, and acetylcholinesterase inhibition. No inhibition was seen for MAO-A and MAO-B at a 1-μM concentration. The IC_{50} for acetylcholinesterase was 6 μM. The maximum human dose of T807 is approximately 13 μg (based on an injected dose of 10 mCi); therefore, the potential for adverse effects resulting from inhibition of any of these CNS targets is low.

4. Discussion

Tau aggregates are a pathological hallmark of AD and are therefore an important target for the development of PET imaging agents and Alzheimer's therapeutics. Our work focuses on small molecules as opposed to peptides or proteins, because they are not only able to pass the blood–brain barrier more easily, but are also capable of binding to tau aggregates selectively relative to aggregates composed of Aβ and α-synuclein [35]. Chemically induced synthetic tau fibrils are not a reliable surrogate for native NFTs,

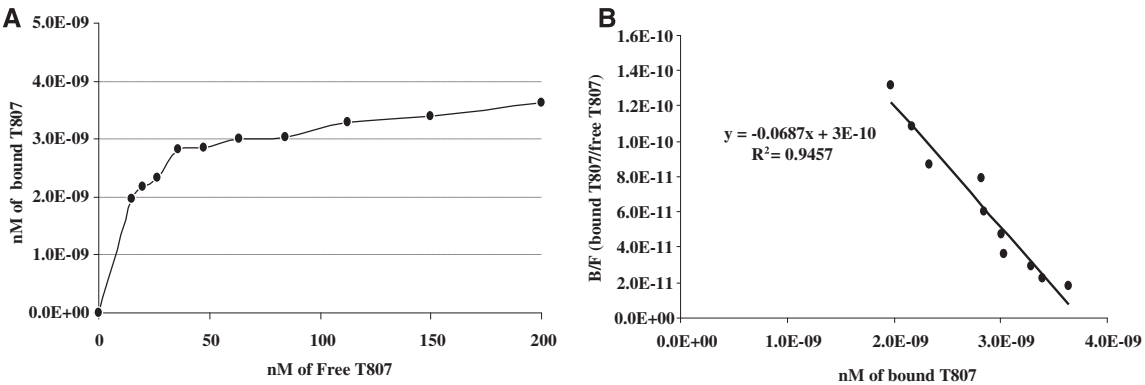

Fig. 5. Dissociation constant (K_d) determination of [^{18}F]T807 binding to native tau aggregates in human Alzheimer's disease brain sections. (A) Native paired helical filament-tau binding of T807. (B) K_d calculation of T807 on brain sections. Scatchard plot analysis for K_d calculation of [^{18}F]T807 binding to native tau aggregates. [^{18}F]T807 binding to native brain tissue with K_d = 14.56 nM.

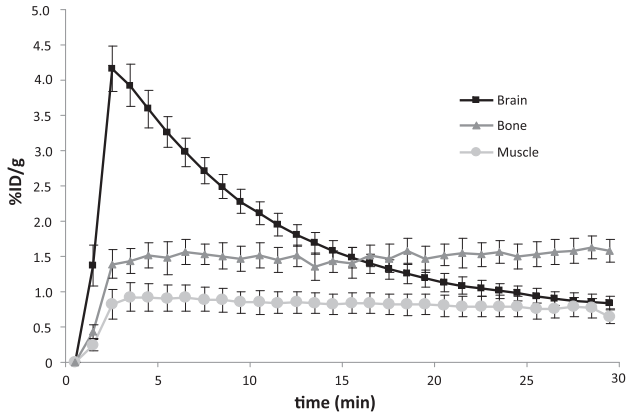

Fig. 6. Kinetics of brain uptake and clearance of [^{18}F]T807 in mouse brains. [^{18}F]T807 showed rapid brain penetration and fast washout in mice (n = 6). Maximal [^{18}F]T807 brain uptake (4.16% ID/g) was observed at 2 minutes after injection of the radiotracer followed by rapid clearance from the brain.

prompting us to use intact brain tissue sections and in vitro autoradiography to evaluate binding properties of small-molecule PHF-tau ligands.

Our studies show that the PET imaging radiotracer [^{18}F]T807 satisfies the criteria required for quantitative imaging of PHF-tau pathology in the human brain, which includes high affinity, selectivity, and lipophilicity [36,37]. [^{18}F]T807 demonstrates high affinity for native tau aggregates and selectivity over Aβ plaques in human AD brain tissues. The K_d value of [^{18}F]T807 binding to PHF-tau is in the nanomolar range as estimated by in vitro saturation binding studies. Because there is more amyloid plaque present in AD brains than NFTs, a high selectivity (>10 fold) for tau tangles over Aβ is essential for obtaining a high signal over background in human PET brain imaging studies [36]. With a selectivity of > 25 fold for PHF-tau over Aβ, as assessed by the autoradiography signal intensity ratios on Aβ$^+$/PHF-tau$^+$ and Aβ$^+$/PHF-tau$^-$ brain sections, [^{18}F]T807 shows potential to be a suitable PHF-tau radiotracer.

Furthermore, [^{18}F]T807 could be produced with high specific radioactivity (9.63 Ci/μmol). PET brain imaging studies with [^{18}F]T807 showed rapid brain penetration and a moderate rate of washout in mice. The average peak percent injected dose per gram in mice is comparable with other amyloid tracers (such as [11C]PiB). The majority of the radiotracer was distributed primarily in three major organs: the kidneys, the bladder, and, to a lesser extent, the liver. Its ability to enter the brain and to clear without appreciable nonspecific binding is a positive feature for a PET brain imaging tracer for PHF-tau protein aggregates.

The biostability percent injected dose per gram values obtained with [^{18}F]T807 in mice were comparable with the percent injected dose per gram data obtained in PK experiments. Although [^{18}F]T807 potentially defluorinates to a minor extent in vivo in mice, the brain homogenate contains only parent signal with no other metabolites detected. To predict possible metabolism in humans, the tracer was incubated with human liver microsomes (data not shown) and was found to be much more stable than with mouse liver microsomes. This is an indication that there might be less metabolism and bone uptake in humans. The potential for off-target binding was assessed further using T807 against a panel of 72 of the most common CNS targets, in which T807 only showed very modest inhibition of human norepinephrine transporter and rabbit monoamine transporter.

We also tested the lead compound in tau transgenic mice, APPSWE-Tau (wild type/hemizygous; Taconic, Hudson, NY), which carry the transgene for the human P301L mutation of the microtubule-associated protein tau gene (data not shown). There was no noticeable difference in retention or maximum uptake between tau transgenic and wild-type mice (data not shown). Similar observations were reported with amyloid imaging agents, such as [^{11}C]PiB, which showed no difference in retention in PS1/APP and PS1 mice. In addition, a very low efficiency for forming high-affinity PiB binding sites during amyloid plaque deposition in vivo in the PS1/APP mouse was also observed [38]. There are six isoforms of tau in human AD brains, including three tau isoforms that have four repeats, and three tau isoforms that have three repeats. In transgenic mice, the P301L mutation only affects the 4R, but not the 3R, tau. Microscopically, PHF-tau in the transgenic mouse brain also looks structurally different from AD human pathology. These differences between human AD and transgenic mice may explain why [^{18}F]T807 binds only to human but not to mouse PHF-tau.

In summary, we report a highly selective and specific PET tracer for in vivo imaging of tau pathologies. The preclinical characterization of [^{18}F]T807 demonstrated high levels of PHF-tau binding affinity, selectivity, and specificity, as well as desirable pharmacokinetic characteristics as a PET tracer for PHF-tau imaging in AD brains. The selective binding to PHF-tau tangles is highlighted by in vitro autoradiographic assays using intact postmortem human brain tissue sections that best reproduce the native tau and other protein aggregates in AD brains.

Table 1
Biodistribution of [^{18}F]T807 in mice

Time, min	Kidneys	Liver	Brain	Muscle	Blood	Plasma	Bone
5	14.99 ± 0.39	4.44 ± 0.16	4.43 ± 0.91	1.04 ± 0.33	0.89 ± 0.03	0.63 ± 0.01	1.37 ± 0.16
15	9.91 ± 1.42	6.32 ± 0.33	1.92 ± 0.06	0.46 ± 0.12	0.68 ± 0.03	0.63 ± 0.04	1.06 ± 0.08
30	5.52 ± 0.91	5.99 ± 0.42	0.62 ± 0.06	0.53 ± 0.14	0.64 ± 0.06	0.71 ± 0.13	0.52 ± 0.17

Data are presented as mean ± standard deviation. The unit of data is percent injected dose per gram.

We are currently testing this PET tracer in Alzheimer's dementia patients and age-matched healthy control subjects to determine its utility as a noninvasive imaging agent for AD. Tau aggregates, even in the absence of Aβ deposits, are characteristic of other progressive neurological diseases such as supranuclear palsy, corticobasal degeneration, Pick's disease, argyrophilic grain disease, frontotemporal dementia, and parkinsonism linked to chromosome 17 [39]. We are currently evaluating the potential of [^{18}F]T807 to bind to these tauopathies and will report the results in due course. This may lead eventually to PET-based methods for improved diagnosis and characterization of dementia, monitoring disease progression, or evaluating therapeutic effectiveness.

RESEARCH IN CONTEXT

1. Systematic review: Molecular imaging of neurofibrillary tangles (NFTs/tau) is a new frontier in Alzheimer's disease (AD) diagnosis. Current NFT/tau imaging efforts have not yet yielded convincing results. We describe a novel and highly selective NFT/tau binder, [^{18}F]T807. For the discovery of this tracer, actual human AD brain sections were used for screening a targeted compound library. Leads were characterized by autoradiography staining and comparison with NFT/tau and β-amyloid immunostaining.
2. Interpretation: [^{18}F]T807 demonstrates high affinity and selectivity to NFT/tau as well as favorable in vivo properties, making this a promising candidate as an NFT/tau imaging agent for AD as well as other tauopathies.
3. Future direction: We are currently testing [^{18}F]T807 in AD dementia patients and age-matched healthy control subjects. The early results in patients are very encouraging. We plan to evaluate the potential of [^{18}F]T807 to bind to other tauopathies, and will report the results in due course.

References

[1] Blennow K, Vanmechelen E, Hampel H. CSF total tau, Abeta42 and phosphorylated tau protein as biomarkers for Alzheimer's disease. Mol Neurobiol 2001;24:87–97.

[2] Sunderland T, Linker G, Mirza N, Putnam KT, Friedman DL, Kimmel LH, et al. Decreased beta-amyloid 1–42 and increased tau levels in cerebrospinal fluid of patients with Alzheimer disease. JAMA 2003;289:2094–103.

[3] Shaw LM, Vanderstichele H, Knapik-Czajka M, Clark CM, Aisen PS, Petersen RC, et al. Cerebrospinal fluid biomarker signature in Alzheimer's disease neuroimaging initiative subjects. Ann Neurol 2009; 65:403–13.

[4] Buerger K, Alafuzoff I, Ewers M, Pirttila T, Zinkowski R, Hampel H. No correlation between CSF tau protein phosphorylated at threonine 181 with neocortical neurofibrillary pathology in Alzheimer's disease. Brain 2007;130:e82.

[5] Mandelkow EM, Mandelkow E. Tau in Alzheimer's disease. Trends Cell Biol 1998;8:425–7.

[6] Itoh N, Arai H, Urakami K, Ishiguro K, Ohno H, Hampel H, et al. Large-scale, multicenter study of cerebrospinal fluid tau protein phosphorylated at serine 199 for the antemortem diagnosis of Alzheimer's disease. Ann Neurol 2001;50:150–6.

[7] Mintun MA, Larossa GN, Sheline YI, Dence CS, Lee SY, Mach RH, et al. [11C]PIB in a nondemented population: potential antecedent marker of Alzheimer disease. Neurology 2006;67:446–52.

[8] Liu J, Kepe V, Zabjek A, Petric A, Padgett HC, Satyamurthy N, et al. High-yield, automated radiosynthesis of 2-(1-{6-[(2-[18F]fluoroethyl)(methyl)amino]-2-naphthyl}ethylidene)malononitrile ([18F] FDDNP) ready for animal or human administration. Mol Imaging Biol 2007;9:6–16.

[9] Johnson AE, Jeppsson F, Sandell J, Wensbo D, Neelissen JA, Jureus A, et al. AZD2184: a radioligand for sensitive detection of beta-amyloid deposits. J Neurochem 2009;108:1177–86.

[10] Verhoeff NP, Wilson AA, Takeshita S, Trop L, Hussey D, Singh K, et al. In-vivo imaging of Alzheimer disease beta-amyloid with [11C] SB-13 PET. Am J Geriatr Psychiatry 2004;12:584–95.

[11] Rowe CC, Ackerman U, Browne W, Mulligan R, Pike KL, O'Keefe G, et al. Imaging of amyloid beta in Alzheimer's disease with 18F-BAY94-9172, a novel PET tracer: proof of mechanism. Lancet Neurol 2008;7:129–35.

[12] Choi SR, Golding G, Zhuang Z, Zhang W, Lim N, Hefti F, et al. Preclinical properties of 18F-AV-45: a PET agent for Abeta plaques in the brain. J Nucl Med 2009;50:1887–94.

[13] Mathis CA, Wang Y, Holt DP, Huang GF, Debnath ML, Klunk WE. Synthesis and evaluation of 11C-labeled 6-substituted 2-arylbenzothiazoles as amyloid imaging agents. J Med Chem 2003; 46:2740–54.

[14] Rowe CC, Ng S, Ackermann U, Gong SJ, Pike K, Savage G, et al. Imaging beta-amyloid burden in aging and dementia. Neurology 2007; 68:1718–25.

[15] Klunk WE, Engler H, Nordberg A, Wang Y, Blomqvist G, Holt DP, et al. Imaging brain amyloid in Alzheimer's disease with Pittsburgh compound-B. Ann Neurol 2004;55:306–19.

[16] Engler H, Forsberg A, Almkvist O, Blomquist G, Larsson E, Savitcheva I, et al. Two-year follow-up of amyloid deposition in patients with Alzheimer's disease. Brain 2006;129:2856–66.

[17] Jack CR Jr, Knopman DS, Jagust WJ, Shaw LM, Aisen PS, Weiner MW, et al. Hypothetical model of dynamic biomarkers of the Alzheimer's pathological cascade. Lancet Neurol 2010; 9:119–28.

[18] Duyckaerts C, Brion JP, Hauw JJ, Flament-Durand J. Quantitative assessment of the density of neurofibrillary tangles and senile plaques in senile dementia of the Alzheimer type: comparison of immunocytochemistry with a specific antibody and Bodian's protargol method. Acta Neuropathol 1987;73:167–70.

[19] Fodero-Tavoletti MT, Okamura N, Furumoto S, Mulligan RS, Connor AR, McLean CA, et al. 18F-THK523: a novel in vivo tau imaging ligand for Alzheimer's disease. Brain 2011;134:1089–100.

[20] Zeng Z, Chen T, Miller P, Connolly B, Selnick H, Pollack S, Sur C, Hamill T. In vitro study on [3H]THK523 binding to brain tissues of Alzheimer's Disease. Presented at the Alzheimer's Association International Conference, Vancouver, BC, Canada. July 14-19, 2012.

[21] Zhang W, Arteaga J, Cashion DK, Chen G, Gangadharmath U, Gomez LF, et al. A highly selective and specific PET tracer for imaging of tau pathologies. J Alzheimers Dis 2012;31:601–2.

[22] Gotz J, Chen F, van Dorpe J, Nitsch RM. Formation of neurofibrillary tangles in P301l tau transgenic mice induced by Abeta 42 fibrils. Science 2001;293:1491–5.

[23] Lewis J, Dickson DW, Lin WL, Chisholm L, Corral A, Jones G, et al. Enhanced neurofibrillary degeneration in transgenic mice expressing mutant tau and APP. Science 2001;293:1487–91.
[24] Ballatore C, Lee VM, Trojanowski JQ. Tau-mediated neurodegeneration in Alzheimer's disease and related disorders. Nat Rev Neurosci 2007;8:663–72.
[25] Stomrud E, Hansson O, Blennow K, Minthon L, Londos E. Cerebrospinal fluid biomarkers predict decline in subjective cognitive function over 3 years in healthy elderly. Dement Geriatr Cogn Disord 2007; 24:118–24.
[26] Duyckaerts C. Looking for the link between plaques and tangles. Neurobiol Aging 2004;25:735–9. discussion 43–6.
[27] Armstrong RA, Myers D, Smith CU. The spatial patterns of plaques and tangles in Alzheimer's disease do not support the 'cascade hypothesis.'. Dementia 1993;4:16–20.
[28] Arriagada PV, Growdon JH, Hedley-Whyte ET, Hyman BT. Neurofibrillary tangles but not senile plaques parallel duration and severity of Alzheimer's disease. Neurology 1992;42:631–9.
[29] Gomez-Isla T, Hollister R, West H, Mui S, Growdon JH, Petersen RC, et al. Neuronal loss correlates with but exceeds neurofibrillary tangles in Alzheimer's disease. Ann Neurol 1997;41:17–24.
[30] Braak H, Braak E. Neuropathological staging of Alzheimer-related changes. Acta Neuropathol 1991;82:239–59.
[31] Chirita CN, Congdon EE, Yin H, Kuret J. Triggers of full-length tau aggregation: a role for partially folded intermediates. Biochemistry 2005;44:5862–72.
[32] Honson NS, Johnson RL, Huang W, Inglese J, Austin CP, Kuret J. Differentiating Alzheimer disease-associated aggregates with small molecules. Neurobiol Dis 2007;28:251–60.
[33] Rojo LE, Alzate-Morales J, Saavedra IN, Davies P, Maccioni RB. Selective interaction of lansoprazole and astemizole with tau polymers: potential new clinical use in diagnosis of Alzheimer's disease. J Alzheimers Dis 2010;19:573–89.
[34] Cheng Y, Prusoff WH. Relationship between the inhibition constant (K1) and the concentration of inhibitor which causes 50 per cent inhibition (I50) of an enzymatic reaction. Biochem Pharmacol 1973; 22:3099–108.
[35] Chang E, Honson NS, Bandyopadhyay B, Funk KE, Jensen JR, Kim S, et al. Modulation and detection of tau aggregation with small-molecule ligands. Curr Alzheimer Res 2009;6:409–14.
[36] Laruelle M, Slifstein M, Huang Y. Relationships between radiotracer properties and image quality in molecular imaging of the brain with positron emission tomography. Mol Imaging Biol 2003;5:363–75.
[37] Pike VW. PET radiotracers: crossing the blood–brain barrier and surviving metabolism. Trends Pharmacol Sci 2009;30:431–40.
[38] Klunk WE, Lopresti BJ, Ikonomovic MD, Lefterov IM, Koldamova RP, Abrahamson EE, et al. Binding of the positron emission tomography tracer Pittsburgh compound-B reflects the amount of amyloid-beta in Alzheimer's disease brain but not in transgenic mouse brain. J Neurosci 2005;25:10598–606.
[39] Lee VM, Goedert M, Trojanowski JQ. Neurodegenerative tauopathies. Annu Rev Neurosci 2001;24:1121–59.